Evaluation of TIG flux welding on the characteristics of stainless steel

H. Y. Huang*[1], S. W. Shyu[2], K. H. Tseng[3] and C. P. Chou[4]

The aim of the present study was to investigate the effect of specific oxide fluxes on the surface appearance, weld morphology, retained δ ferrite content, hot cracking susceptibility, angular distortion and mechanical properties obtained with the tungsten inert gas (TIG) process applied to the welding of 5 mm thick austenitic stainless steel plates. An autogenous gas tungsten arc welding process was applied to stainless steels through a thin layer of activating flux to produce a bead on plate welded joint. The MnO_2 and ZnO fluxes used were packed in powdered form. The experimental results indicated that the 80% MnO_2–20% ZnO mixture can give full penetration and also a satisfactory surface appearance for type 304 stainless steel TIG flux welds. TIG welding with MnO_2 and/or ZnO can increase the measured ferrite number in welds, and tends to reduce hot cracking susceptibility in as welded structures. It was also found that TIG flux welding can significantly reduce the angular distortion of stainless steel weldments.

Keywords: Angular distortion, δ ferrite, Hot cracking susceptibility, Stainless steel, TIG flux

Introduction

Fabrication of metal structures in space will require extensive use of various metal joining processes. The tungsten inert gas (TIG) welding process is one of several methods being considered for this purpose. The TIG welding technique is widely accepted for its ability to produce higher quality welds in a variety of materials. Advantages of this process include higher quality weld deposits, precise control of welding parameters, and relatively lower equipment costs. Consequently, the practical TIG welding technique is used in various industries to produce single pass full penetration welds and the root passes of multipass welds.

Improvements in weld penetration capability have long been sought in many joining processes. One of the most notable examples is the use of activating flux with the TIG welding process.[1–5] TIG flux welding based on various oxides, halides and metal powder compounds is being used on an increasing scale in industry. This technique makes it possible to intensify conventional TIG welding for joining thickness of 8–10 mm by single pass welds, with no edge preparation, instead of multipass procedures. There are significant increases in weld penetration capability, as much as 300%, compared to conventional practices.[1,2,6,7]

This concept of using a flux with TIG welding processes to increase weld penetration was invented in the 1960s by researchers at the Paton Electric Welding Institute (PWI) in the Ukraine.[8] Although the PWI has published information regarding the use of the activating flux, only a few data are available in the open literature about the activating flux composition. Such data are very important to determine the weld penetration improvement function of the activating flux. In the present work, a specific activating flux composition suitable for autogenous TIG welds of stainless steel was developed and used to enhance penetration capability and weld quality.

Experimental procedure

Austenitic type 304 stainless steel with the chemical composition and mechanical properties listed in Table 1 was used. Plates 5 mm in thickness were cut into strips of size 150×150 mm, which were roughly polished with 400 grit abrasive paper to remove surface impurities, and then cleaned with acetone. Activating flux composed of MnO_2–ZnO powder mixtures, in a layer less than 0·2 mm thick, was applied to the surface of the joint to be welded by means of a brush before TIG welding. Figure 1 is a schematic diagram of TIG welding with the activating flux. Autogenous (no filler metal added) TIG welding was conducted on type 304 stainless steels to produce a bead on plate weld. A machine mounted torch with a standard 2% thoriated tungsten electrode (3·2 mm diameter) was used. The electrode tip configuration was a blunt point with a 60° angle. Welding parameters used in the present study are given in Table 2. During welding, a CCD camera system was used to observe and record images of the welding arc and the molten pool.

[1]Department of Mechanical Engineering, National Chiao Tung University, Hsinchu 300, Taiwan
[2]Department of Mechanical Engineering, National United University, Miaoli 360, Taiwan
[3]Welding Technology Section, Metal Industries Research & Development Centre, Kaohsiung 811, Taiwan
[4]Department of Mechanical Engineering, National Chiao Tung University, Hsinchu 300, Taiwan

*Corresponding author, email hyhuang.me90g@nctu.edu.tw

Published by Maney on behalf of the Institute
Received 15 November 2004; accepted 17 March 2005
DOI 10.1179/174329305X48329

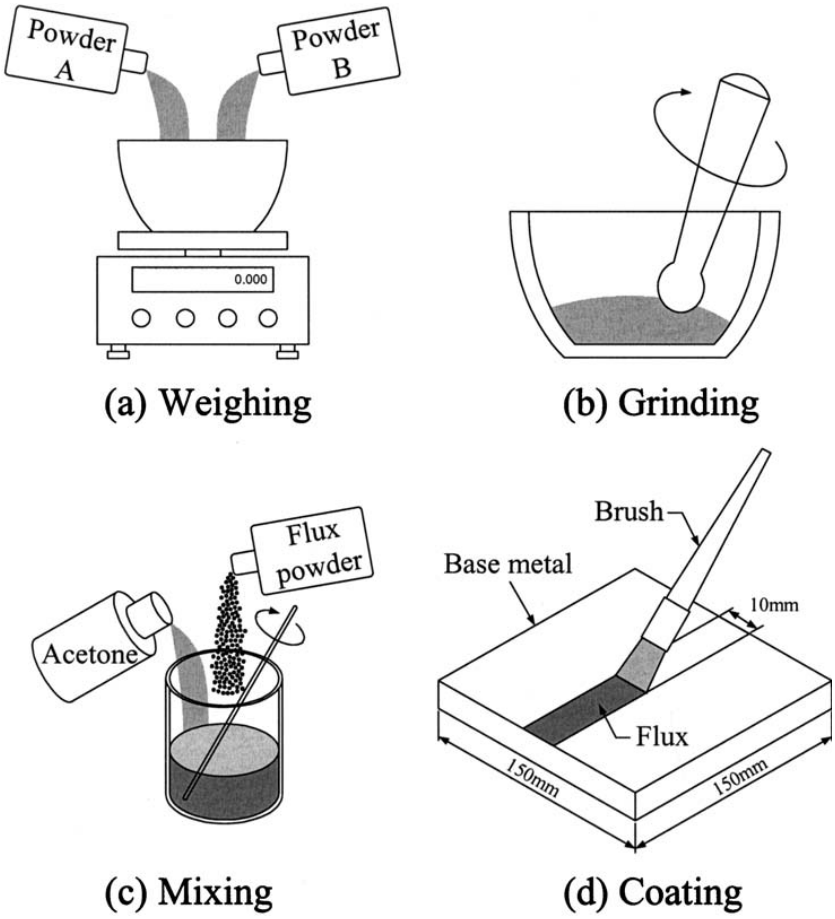

a Weighing; *b* Grinding; *c* Mixing; *d* Coating

1 Schematic diagram of TIG welding with the activating flux

The ferrite number (FN) was measured using a calibrating magnetic instrument with a Ferritscope M10B-FE. To minimise the measured errors due to weldment inhomogeneity, the average value of seven measurements from different locations along the as welded surface was recorded.

Figure 2 is a schematic diagram of welding distortion measurement. A position fixed hole was drilled at the back of points P_1, P_2 and P_3, and a pillar was attached to each hole. Three pillars (one stable, the other two adjustable) were used to adjust the horizontal level. Prior to measuring, five sets of measuring positions were determined on both the left side (A–E) and right side (F–J) of the as welded surface along the y-axis. During the measurement, the stage was moved along the x-axis by 50 mm, and a vertical displacement Z was obtained. The angular distortion value θ can be derived from the equation

$$\theta = \tan^{-1}\frac{Z}{50}$$

Finally, the five positions on either side of the welds were averaged, and then added together to give the angular distortion value.

In the present work, the hot cracking susceptibility was evaluated by the spot varestraint test.[9–11] The welding conditions were 80 A arc current with 8 s arc time on 3 mm thick plates, and the arc length was maintained at 1·6 mm. Hot cracking occurred in both the weld metal and heat affected zone (HAZ). In this evaluation of the hot cracking susceptibility, the total crack length in the weld metal was normalised on the basis of the molten pool diameter. Figure 3 shows the spot varestraint test method in a schematic form.

Transverse tensile and Vickers hardness tests were used to examine the metallurgical properties of TIG flux stainless steel weldments. Transverse tensile tests of three specimens from each weld procedure combination were used to determine the tensile strength of the weldments. The configuration and size of the tensile specimens were in accordance with ASTM E8. Vickers hardness profiles across the weld metal, HAZ and partial base metal were measured under a load of 1·96 N for 15 s along the weld centreline. An optical microscope was used to measure the dimensions of the weld bead geometry (weld penetration, bead width and HAZ range). All metallographic specimens were prepared by mechanical lapping, grinding and polishing to a 0·3 μm finish, followed by etching in a solution of 10 g $CuSO_4$–50 mL HCl–50 mL H_2O.

Table 1 Chemical composition (wt-%, balance Fe) and mechanical properties of experimental austenitic stainless steel

C	Si	Mn	P	S	Cr	Ni	Yield strength, MPa	Elastic modulus, GPa	Poisson's ratio
0·07	0·51	1·30	0·026	0·013	18·7	8·16	290	193	0·25

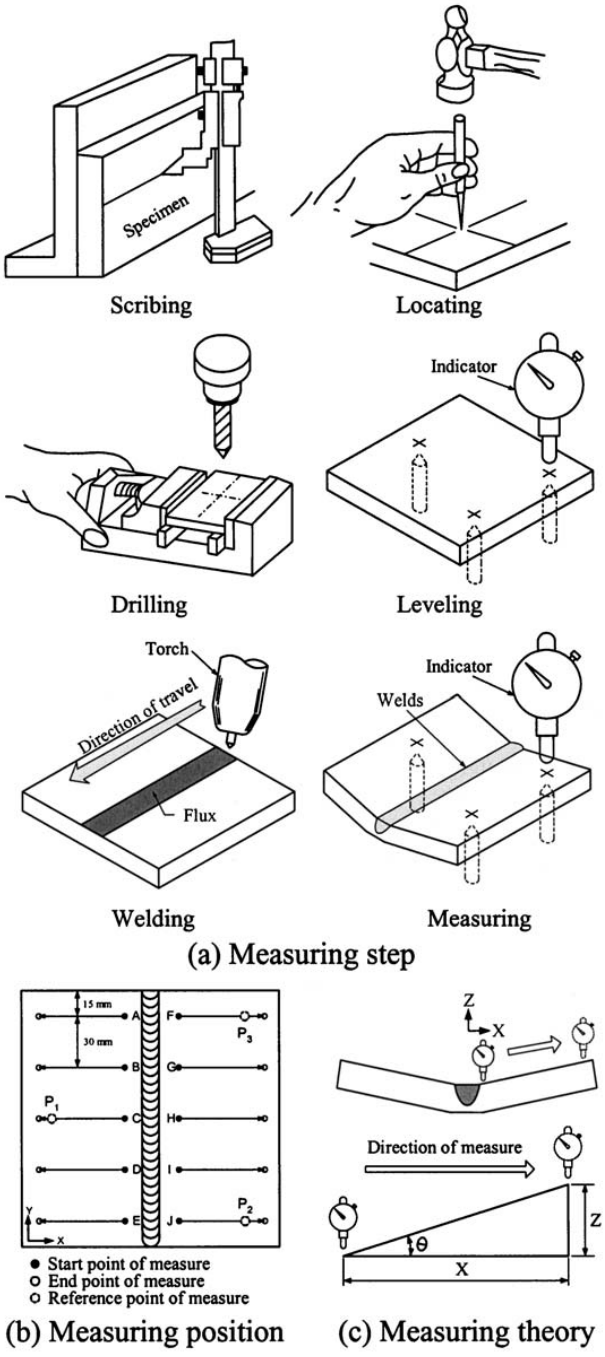

a Measuring step; *b* Measuring position; *c* Measuring theory

2 Schematic diagram of welding distortion measurement

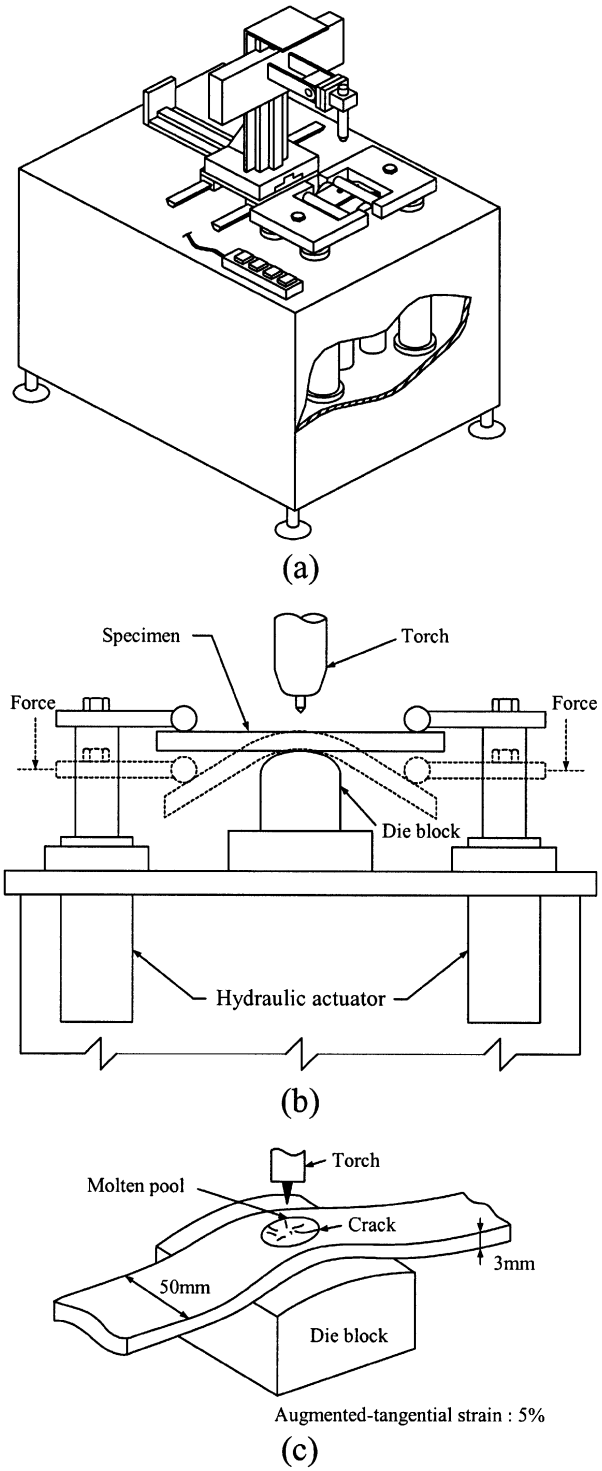

3 Schematic diagram of spot varestraint test

Results and discussion

Effect of activating fluxes on surface appearance

Figure 4 shows the surface appearance of type 304 stainless steel TIG flux welds produced with various flux compositions. Figure 4*a* shows the results of the 20% MnO_2–80% ZnO mixture, which produced excessive slag. Figure 4*b* shows that few slag and undercut defects were produced with use of the 40% MnO_2–60% ZnO mixture. Figure 4*c* shows no slag defects, but undercut defects were still produced with use of the 60% MnO_2–40% ZnO mixture. Figure 4*d* shows the satisfactory surface appearance of TIG flux stainless steel welds obtained with use of the 80% MnO_2–20% ZnO mixture.

Table 2 Welding parameters for autogenous TIG welding experiments

Welding current	125 A
Travel speed	75 mm min^{-1}
Arc length	3 mm
Argon flowrate	10 L min^{-1}

Effect of activating fluxes on weld morphology

Figure 5 shows the cross-sections of TIG welds produced without flux and with various flux compositions in 5 mm thick stainless steel. There was significant

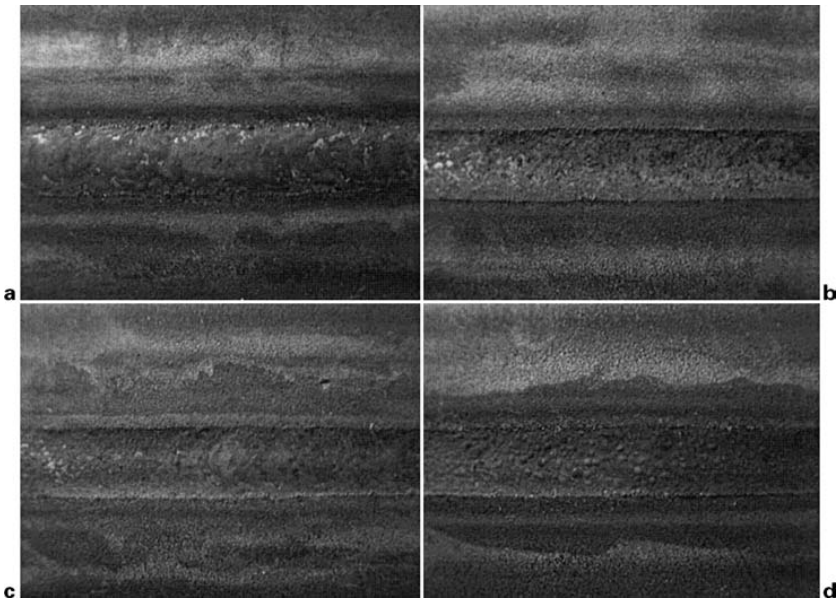

a 20% MnO_2+80% ZnO; *b* 40% MnO_2+60% ZnO; *c* 60% MnO_2+40% ZnO; *d* 80% MnO_2+20% ZnO

4 Effect of activating fluxes on surface appearance

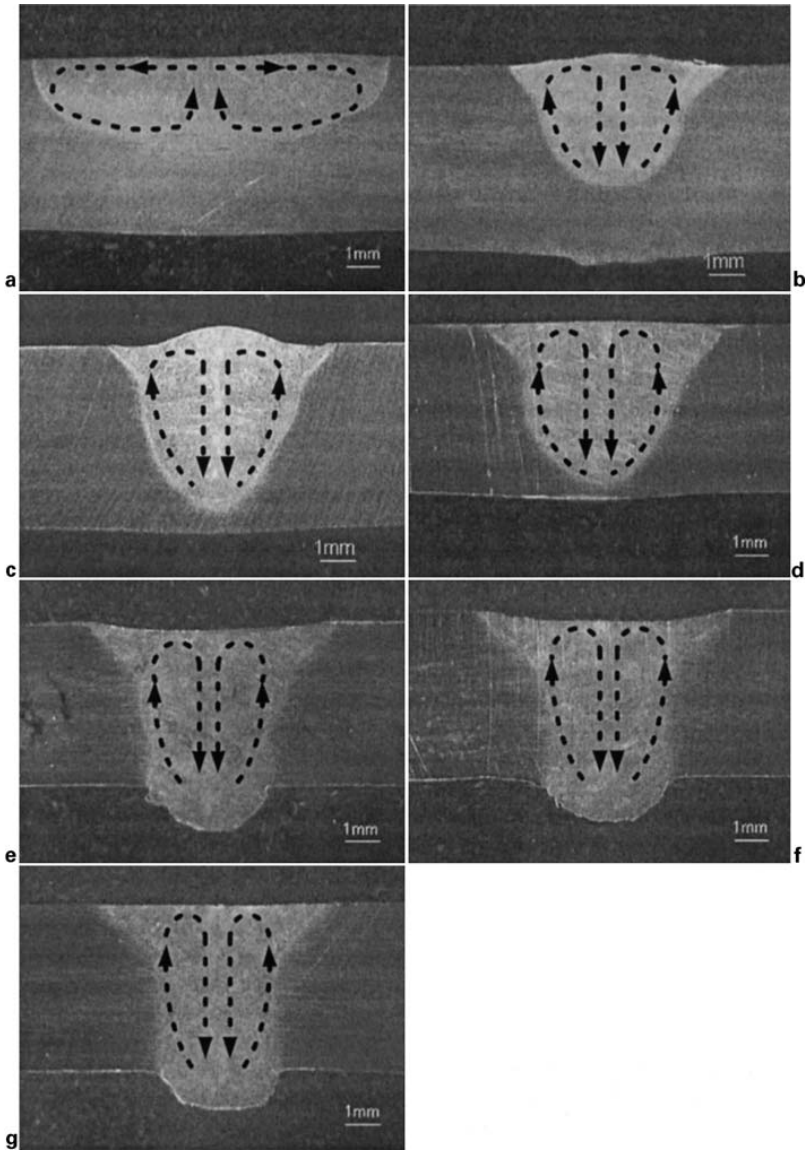

a Without flux; *b* 100% MnO_2; *c* 100% ZnO; *d* 20% MnO_2+80% ZnO; *e* 40% MnO_2+60% ZnO; *f* 60% MnO_2+40% ZnO; *g* 80% MnO_2+20% ZnO

5 Effect of activating fluxes on weld morphology

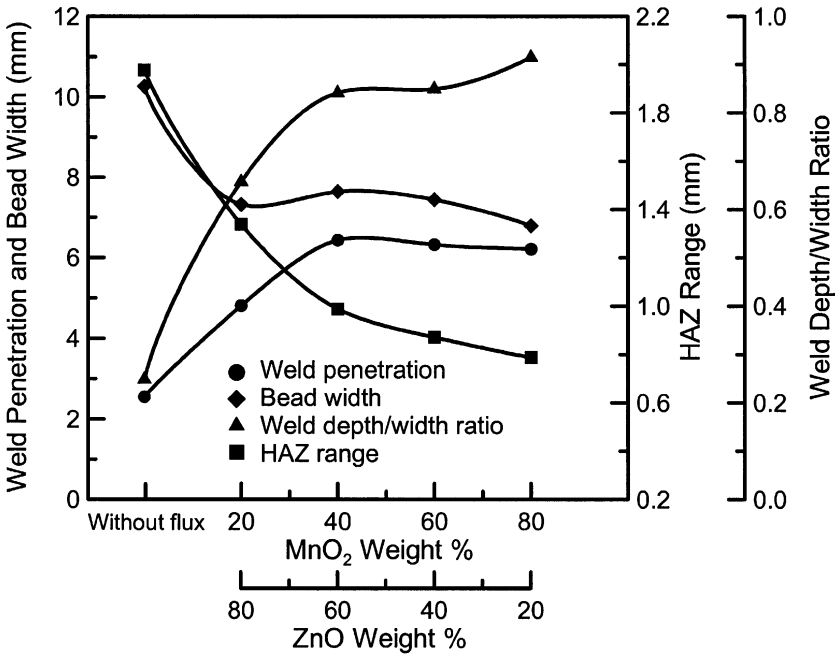

6 Characteristics of TIG weld geometry produced with various flux compositions

variation in the penetration and bead width of the welds. According to work by Heiple,[12–16] the direction of fluid flow can affect the weld morphology. For TIG welding, the surface tension will be greatest at the edge of the weld pool and lowest in the hottest part of the weld pool near the centre under the arc. The surface tension gradient therefore produces fluid flow outwards from the centre of the weld pool surface, as indicated in Fig. 5*a*, resulting in a relatively wide and shallow weld bead. The addition of surface active elements to molten metals can drastically change the temperature dependence of the surface tension. For TIG flux welding, the surface tension is highest near the centre (hotter) region of the weld pool. Fluid flow will be inwards along the surface of the weld pool towards the centre and then down, as indicated in Fig. 5*b–g*, and tend to increase the weld penetration.

Figure 6 shows the characteristics of TIG weld geometry produced with various flux compositions. The increases in weld penetration and the decrease in bead width are significant with use of the activating flux, which is composed of MnO_2 and/or ZnO powder mixture. In the present study, the 40% MnO_2–60% ZnO mixture led to the greatest improvement in penetration capability, up to 250%, compared with the conventional TIG process for type 304 stainless steel. It should be mentioned that the 80% MnO_2–20% ZnO mixture can give full weld penetration and satisfactory surface appearance.

It can also be seen in Fig. 6 that TIG welding with MnO_2 and/or ZnO can increase the weld depth/width ratio and reduce the HAZ range. According to previous investigations,[17,18] a greater weld depth/width ratio and a narrower HAZ range are characteristics of the

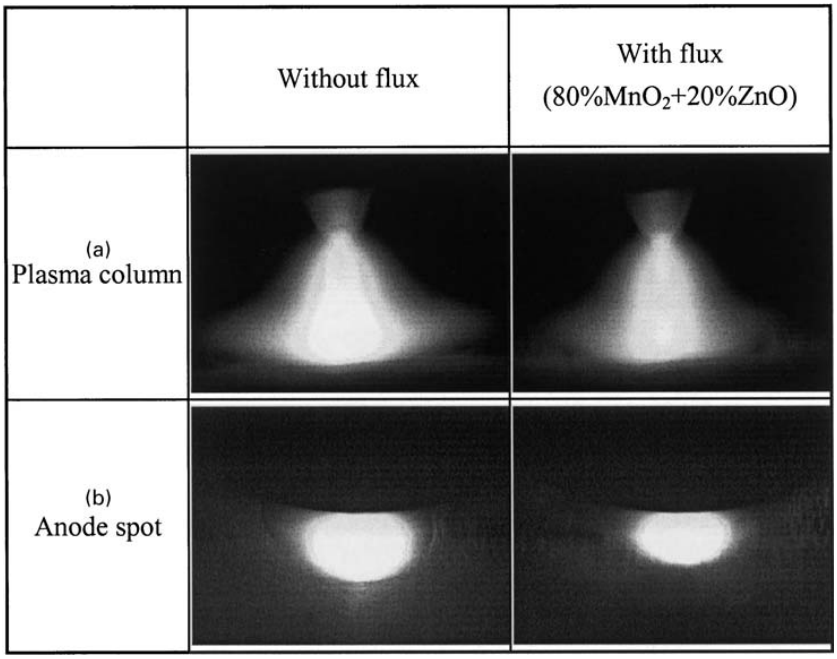

7 Effect of TIG welding without and with flux on plasma column and anode spot

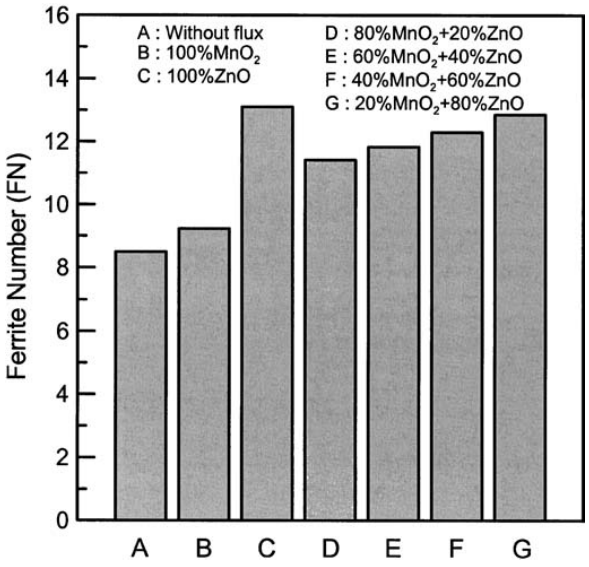

8 Effect of activating fluxes on retained δ ferrite content

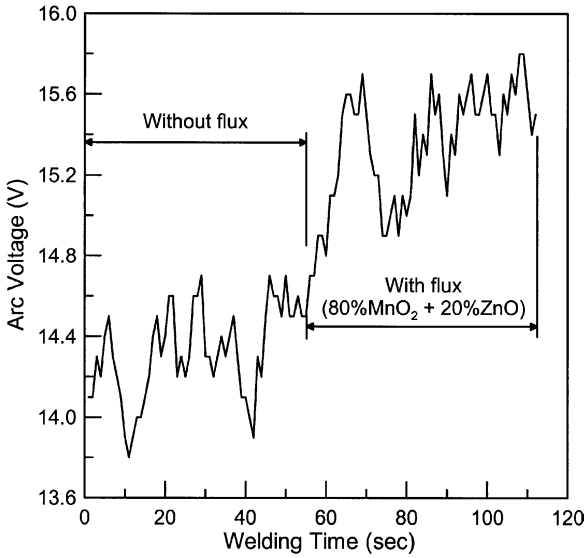

9 Effect of TIG welding without and with flux on arc voltage

increased energy density of the welding heat source, and thereby the high degree of energy concentration during TIG flux welding process.

Mechanism for increased TIG flux weld depth/width ratio

The major effect of the activating flux appears to be on the characteristic of the arc rather than on the chemistry of the weld pool.[1] In arcing without and with flux (shown in Fig. 7), the central part of the arc shows clearly in a glowing zone occupying almost the entire arc length. This zone is regarded as the plasma column (current carried by the electrons and ions produced by thermal ionisation of the shielding gas). It can be seen in Fig. 7*a* that the TIG flux welding arc shows a constriction in plasma column diameter compared with the conventional TIG welding arc at the same current level. Constriction of the plasma column increases the current density in the anode root, and a more focused arc increase in the penetration of TIG flux welds can be achieved compared with conventional TIG welds.

Other factors, such as anode spot, can also influence weld pool formation. Because the conductivity of the flux is much lower than that of the metal vapours, and its melting point is higher than that of the weld metal, the metal evaporation will be only generated in the central regions of the arc, where the temperature is higher than the dissociation temperature of the flux atoms, leading to a reduction in the area of the anode spot. It can be seen in Fig. 7*b* that the TIG flux molten pool shows a reduction in the anode spot area compared with the conventional TIG molten pool at the same current level.

On the basis of the present results, it is considered that the plasma column and anode spot play a major role in determining TIG flux weld geometry. Physically constricting the plasma column and reducing the anode spot will not only produce a narrower bead width but also increase the weld penetration when using a TIG flux welding process.

Effects of TIG flux welding on retained δ ferrite content

The weld metal microstructure in all the welds consisted of ferrite in an austenitic matrix. The measured FN of 304 stainless steel welds as a function of MnO_2 and/or ZnO application to TIG welding is presented in Fig. 8. When autogenous TIG welding with MnO_2 and/or ZnO is used, the measured FN in weld metals is increased. In type 304 stainless steel welds, the FN was increased to 9·3 from its initial value of 8·5 by use of 100% MnO_2. When 100% ZnO was used, the retained δ ferrite content in type 304 stainless steel welds was increased to 13·1 FN. This result is related to the heat input during TIG welding without and with flux. The effect of TIG welding without and with flux on the arc voltage is shown in Fig. 9. The welding current was maintained at constant value, and it was found that the arc voltage increases when the TIG flux welding process was used. Since the calculated heat input is proportional to the measured arc voltage, applied activating flux has the positive effect of increasing the heat input in welding fabrication. Because this higher heat input can increase the peak temperature of the weld metal and reduce its cooling rate, the retained δ ferrite content in type 304 stainless steel weld metal is increased.[19,20]

Effects of TIG flux welding on hot cracking susceptibility

Activating flux has a great influence on hot cracking susceptibility. Figure 10 shows the effect of TIG welding without and with flux on hot cracking susceptibility of type 304 stainless steel weld metals. The experimental results clearly indicated a reduction in measured total crack length in weld metals with use of the TIG flux welding process. Two explanations were proposed to explain the beneficial effect of the retained δ ferrite structure in reducing hot cracking susceptibility. The first explanation is based on the fact that δ ferrite has a greater high temperature ductility than that of the austenite, and therefore δ ferrite within the austenitic matrix can moderate the action of thermal stress during welding. The second explanation is related to the fact that hot cracking susceptibility is reduced because the body centred cubic ferrite structure has a smaller coefficient of thermal expansion than that of the face

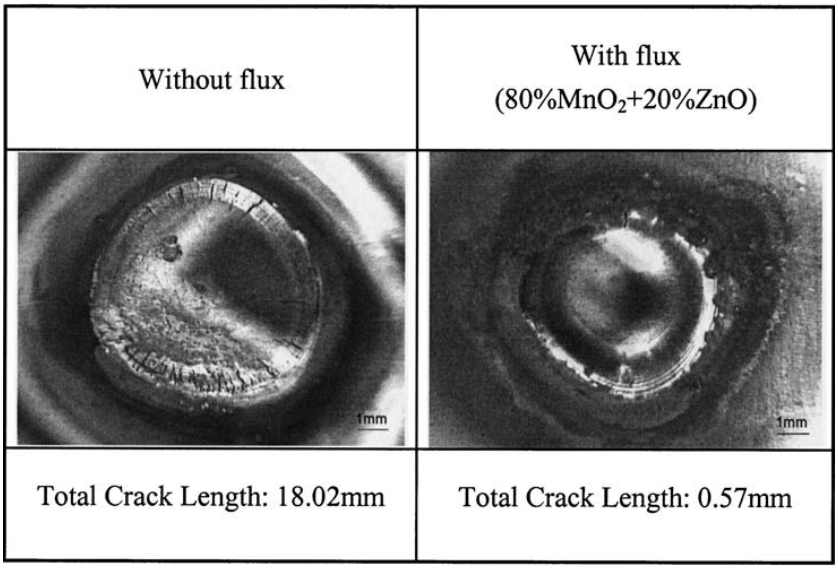

10 Effect of TIG welding without and with flux on hot cracking susceptibility

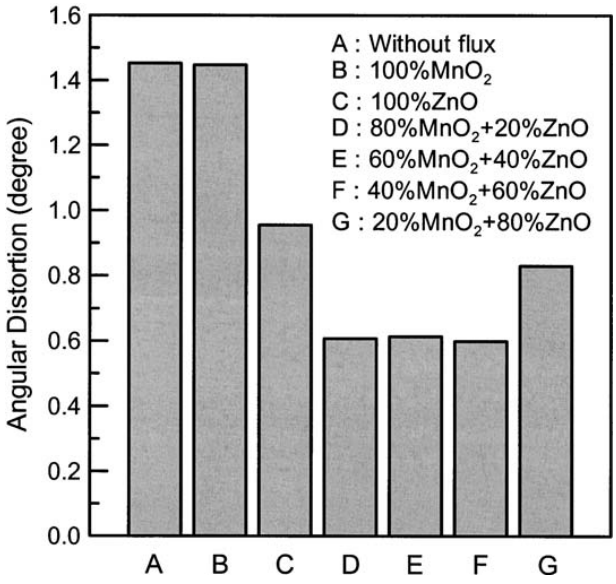

11 Effect of TIG welding without and with flux on angular distortion

centred cubic austenite structure, and thereby shrinkage stresses during cooling are reduced. When TIG welding with MnO_2 and/or ZnO is used, the retained δ ferrite content in weld metals is increased, and has a beneficial effect in reducing the hot cracking susceptibility of austenitic stainless steel welds.

Effects of TIG flux welding on angular distortion

Uneven heating through the thickness during welding of a joint causes non-uniform thermal strains that result in angular distortion. The value of angular distortion depends on several factors, including (i) the relative penetration, and (ii) the shape and dimensions of welds.[21] The effect of TIG welding without and with flux on angular distortion of a type 304 stainless steel weldment is shown in Fig. 11. When autogenous TIG welding with MnO_2 and/or ZnO is used, it can be seen that the angular distortion of the weldment is decreased. Because of a high degree of energy concentration during the TIG flux welding process, both the molten pool and the HAZ are reduced. This contributes to a reduction in the quantity of supplied heat and, in consequence, prevents overheating of the metal; this reduces the incidence of thermal strains due to shrinking (including angular), and therefore the angular distortion of austenitic stainless steel weldments can be reduced.

Effect of TIG flux welding on mechanical properties

Table 3 presents the experimental results for mechanical properties of weldments with and without the fluxes. It can be clearly seen that welds produced by using the TIG flux welding process exhibit equal or better mechanical properties (including strength, ductility, and hardness) than those of autogenous TIG welds deposited without using the flux.

Conclusions

1. In the present study, the 80% MnO_2–20% ZnO mixture can give full weld penetration and also a satisfactory surface appearance with type 304 stainless steel TIG flux welds.

2. The plasma column and anode spot play a major role in determining TIG flux weld geometry. Physically

Table 3 Mechanical properties test results

			Hardness, HV		
	UTS, MPa	Elongation, %	Weld metal	HAZ	Base metal
Without flux	605·42	37·93	181·9	182	183·1
With flux (80% MnO_2–20% ZnO)	645·32	38·85	185·5	182·8	183·2

constricting the plasma column and reducing the anode spot will not only produce a narrower bead width but will also increase weld penetration when using the TIG flux welding process.

3. Since TIG flux welding can increase the arc voltage, the amount of heat input per unit length in a weld is also increased, and therefore the retained δ ferrite content in austenitic stainless steel welds will be increased. As a result, the hot cracking susceptibility in as welded structures is reduced.

4. TIG flux welding can increase the weld depth/width ratio and reduce the HAZ range, which are characteristics of a high degree of energy concentration during the TIG flux welding process; the angular distortion of austenitic stainless steel weldments can therefore be reduced.

References

1. W. Lucas and D. Howse: *Weld. Met. Fabr.*, 1996, **64**, (1), 11–17.
2. T. Paskell, C. Lundin and H. Castner: *Weld. J.*, 1997, **76**, (4), 57–62.
3. M. Tanaka, T. Shimizu, H. Terasaki, M. Ushio, F. Koshi-ishi and C.-L. Yang: *Sci. Technol. Weld. Joining*, 2000, **5**, (6), 397–402.
4. M. Kuo, Z. Sun and D. Pan: *Sci. Technol. Weld. Joining*, 2001, **6**, (1), 17–22.
5. G. Dinechin, C. Chagnot, F. Castillan, O. Blanchot and D. Baude: *Weld. Int.*, 2002, **16**, (9), 720–728.
6. P. C. J. Anderson and R. Wiktorowicz: *Weld. Met. Fabr.*, 1996, **64**, (3), 108–109.
7. T. Paskell, C. Lundin and D. Castner: *Weld. J.*, 1997, **76**, (4), 57–62.
8. S. M. Gurevich and V. M. Zamkov: *Avt. Svarka*, 1966, **12,** 13–16.
9. T. Ogawa and E. Tsunetomi: *Weld. J.*, 1982, **61**, (3), 82–93.
10. J. A. Brook: *Weld. J.*, 1974, **53**, (11), 517–523.
11. P. W. Turner and C. D. Lundin: *Weld. J.*, 1970, **49**, (12), 579–587.
12. C. R. Heiple and J. R. Roper: *Weld. J.*, 1981, **60**, (8), 143–145.
13. C. R. Heiple and J. R. Roper: *Weld. J.*, 1982, **61**, (4), 97–102.
14. C. R. Heiple, J. R. Roper, R. T. Stagner and R. J. Aden: *Weld. J.*, 1983, **62**, (3), 72–77.
15. C. R. Heiple and P. Burgardt: *Weld. J.*, 1985, **64**, (6), 159–162.
16. P. Burgardt and C. R. Heiple: *Weld. J.*, 1986, **65**, (6), 150–155.
17. K. H. Tseng and C. P. Chou: *Sci. Technol. Weld. Joining*, 2001, **6**, (3), 149–153.
18. K. H. Tseng and C. P. Chou: *J. Mater. Process. Technol.*, 2002, **123**, 346–353.
19. K. H. Tseng and C. P. Chou: *Sci. Technol. Weld. Joining*, 2002, **7**, (1), 57–62.
20. C. J. Long and W. T. Delong: *Weld. J.*, 1973, **52**, (7), 281–297.
21. V. I. Pavlovsky and K. Masubuchi: *Weld. Res. Counc. Bull.*, 1994, **388**, 44–48.